IJMPR 2020, 4(2), 91-96

International Journal of Modern Pharmaceutical Research
www.ijmpronline.com

ISSN: 2319-5878
IJMPR
Review Article
SJIF Impact Factor: 5.273

NOVEL INHIBITOR FOR COVID-19 FROM ZINC NANO-BASED AZA-PC AND CQDS

Fadi Ibrahim*

Department of Chemistry, Saad Bin-Alrabee Alansari School Kuwait.

Received on: 26/02/2020
Revised on: 17/03/2020
Accepted on: 06//04/2020

***Corresponding Author**
Fadi Ibrahim
Department of Chemistry, Saad Bin-Alrabee Alansari School Kuwait.

ABSTRACT

In this article, the antiviral activity of seven different carbon quantum dots (CQDs) with Azaphthalocyanin (Az-Pcs) for the treatment of human coronavirus infections was investigated. Az-Pcs used to adsorb UV light and concentrate it to CQDs to avoid destruction of tissue and cells by high energy. The first generation Az- Pcs-CQDs antiviral with nanostructures showed a concentration-dependent virus inactivation with an expected estimated EC50 of 50±8 μ gmL-1. The underlying mechanism of action of these Az-Pcs-CQDs could be due to interaction of the functional groups of the CQDs with COVID-19 entry receptors; surprisingly, an equally large inhibition activity was observed at the viral replication step. Az-Pcs with boronic acid derivatives have been proposed as low toxicity agents for inhibiting the entry various viruses. The underlying mechanism of action of these CQDs was revealed to be the CQDs interaction with the COVID-19 S-protein. The antiviral activity of Az-Pcs-CQDs with different Zn nano-size need to be evaluated on Huh-7 cell monolayers infected with COVID-19.

KEYWORDS: COVID-19; antiviral activity; Zinc nanoparticles; carbon quantum dots (CQDs); UV light; Surface plasmon resonance; Atomic force microscopy; Boronic acid Aza-Pc.

INTRODUCTION

Anticoronavirus therapy is however challenging, as coronaviruses are biologically diverse and rapidly mutating. The strong and stable green light emission of (CQDs) could be synthesized successfully by the one-pot of hydrothermal method from lemon juice. In particular, intensity of the CQDs increases with increasing hydrothermal temperature and time. In addition, CQDs diluted by polar solvents induced stronger luminescence than did the pure CQDs. The obtained CQDs having strong, inert, and stable luminescent properties would be particularly important for potential applications in optoelectronics and bioimaging. These results suggest that the CQDs have potential application in optoelectronics and bioimaging. nanotechnology does have a solution for almost every problem we face, including now-struggling global health: a nanoparticle-based coronavirus vaccine was successfully developed. The ongoing coronavirus outbreak in Wuhan, China, causing rising death tolls, is a wake- up call for global health, in so far as many researchers have turned their focus to this growing threat. In this work, A theoretical study of the antiviral activity of Aza-Pc contain nano-zinc and CQDs for the treatment of human coronavirus infections was investigated. In the last 10 years[1,2] the field of molecular diagnostics has witnessed an explosion of interest in the use of nanomaterials in assays for gases, metal ions, and DNA and protein markers for many diseases. Intense research has been fueled by the need for practical, robust, and highly sensitive and selective detection agents that can address the deficiencies of conventional technologies. Chemists are playing an important role in designing and fabricating new materials for application in diagnostic assays.[3,4] Coronaviruses are a group of viruses that attack the upper and lower respiratory tracts in humans and cause a range of illnesses from the common cold to more serious forms such as severe acute respiratory syndrome (SARS) and the Middle East respiratory syndrome (MERS) which are life-threatening.[5-7] Virions of coronavirus are in the form of spheres with an average diameter of 125 nm. They have a viral envelope and a positive-sense single-stranded RNA genome. Virus particles of coronavirus have four types of structural proteins, namely spike (S), membrane (M), envelope (E), and nucleocapsid (N) proteins, among which the S-protein has a crucial role in attaching the virus to its host's cells and enabling it to enter the cells; thus, an effective way of fighting this virus could be targeting the S protein's mechanism of action by developing special drugs and inhibiting compounds. Recently, a group of researchers from the University of Lille, France, and Ruhr-University Bochum, Germany, showed that the CQDs functionalized with boronic acid ligands interfered with the function of coronavirus's S protein and significantly inhibited its entry into the host cells.[8-10] Their studies demonstrated that the addition of these nanomaterials to the cell culture medium, before and during infection with coronavirus, considerably reduced the infection rate of the cells.[11-14] Surprisingly, after one viral life cycle –

which is 5.5 hours for coronavirus – a great inhibition activity was also observed at the viral replication step. These CQDs with an average diameter of 10 nm and excellent solubility in water can be perfect candidates for winning the battle against coronavirus, because they easily enter the cell through endocytosis and interact with the virus's protein, thereby preventing viral genome replication.[1] Given their high specific surface area of Aza-Pcs and the possibility of being functionalized with a wide range of functional groups, nanomaterials such as zinc nanoparticles and carbon quantum dots (CQDs) are standout choices for interacting with viruses and preventing their entry into cells Figure 1.

Figure 1: Influence of Az-Pcs-CQDs on binding of COVID-19 to cells and inhibition of protein S receptor interaction.

Influence of Aza-Pcs, Zinc nanomaterial of (10, 20 and 30 nm) and CQDs in inhibition of protein S receptor interaction and inhibition of COVID-19 RNA genome replication. In this work, a potential of functional carbon quantum dots (CQDs) as inhibitors of host cells infection by coronavirus (Figure 1). Boronic acid Aza-Pc CQDs were able to inhibit, for example, COVID-19 entry by suppressing syncytium formation. The size of a nanomaterial can be an advantage over a bulk structure, simply because a target binding event involving the nanomaterial can have a significant effect on its physical and chemical properties, thereby providing a mode of signal transduction not necessarily available with a bulk structure made of the same material. CQDs have received considerable attention in bioimaging because of their highly biocompatibility, luminescent properties, and sphere-shaped nanoparticles.[15,16] However, short excitation wavelengths of high energy will cause the destruction of tissue and cells which limit its application in bioimaging and biomedicine. Recently, CQDs were synthesized successfully in our laboratory by the hydrothermal treatment of lemon juices.[17] The results show that CQDs had strong green light emission with quantum yield in the range of 14.86 to 24.89% as a function of hydrothermal temperatures. Furthermore, light emission that is dependent on hydrothermal time, aging of precursor, and diluted solvent was observed derived from apple juice emit a wavelength of 428nm with a quantum yield of 6.4% under the excitation of ultraviolet light of 340nm.[18] In addition to DNA hybridization-promoted nanoparticle aggregation, others demonstrated that hybridization reactions involving oligonucleotide-modified zinc Aza-Pc nanoparticles that do not result in aggregate assembly can result in measurable optical changes that correlate with target concentration. This unique study reveals that boronic acid functions can be responsible for the anti-HCoV activity. CQDs derived from citric acid/ethylenediamine and further conjugated by chemistry with boronic acid functions display an effective CQDs interaction with the protein anti-virus action with large inhibition activity was observed at the viral replication step.

Synthesis of Aza-Pcs

Symmetrically substituted metallo Aza-Pc were prepared by cyclotetramisation of the 5,6-(2,6-diisopropylphenoxy)-pyrazine-2,3-dicarbonitrile in dry quinoline, catalyzed by anhydrous cobalt acetate, nickel acetate, and zinc acetate respectively. The other symmetrically substituted Aza-Pcs were prepared also by cyclotetramisation of the 5,6-(2,6-diphenyllphenoxy)-pyrazine-2,3-dicarbonitrile in dry quinoline, catalyzed by anhydrous cobalt acetate, nickel acetate, and zinc acetate respectively. as shown in Scheme (1).

Metal free Aza-Pcs were prepared by cyclotetramisation under basic conditions of 5,6-(2,6-diisopropylphenoxy)-pyrazine-2,3-dicarbonitrile, and of the 5,6-(2,6-diphenyllphenoxy)-pyrazine-2,3-dicarbonitrile in dry quinoline, respectively. Each of the Aza-Pcs gave a satisfactory spectroscopic analysis (^{1}H NMR, UV/VIS, IR, Elemental analysis and mass spectroscopic (MALDI)

results that were consistent with the proposed structures. In particular, a well-defined shape (i.e. isolated Aza-Pc cores) ^{1}H NMR spectrum was obtained for Aza-Pc under normal conditions (e.g. 25 °C, in $CDCl_3$). In these conditions, normal Pcs usually give highly broadened spectra due to aggregation. In order to prevent self-association of the Aza-Pc unit, the substituents should adopt positions relative to Aza-Pc ring in which they can enforce isolation of the Aza-Pc macrocycle in the solid state. The side-chains lie perpendicular to the plane of the macrocycles described. It was expected that these materials would exhibit enhanced solubility and influencing the molecular packing of Aza-Pc in the solid state. The substituted groups to lie out of the plane of the macrocycle and consequently result in the isolation of the Aza-Pc core. The crude product was recrystallized from n-Hexane to get (**1**) with (62%) yield. The ^{1}H NMR, MS and elemental analysis of (**1**) provided support for the expected structure (see experimental section).

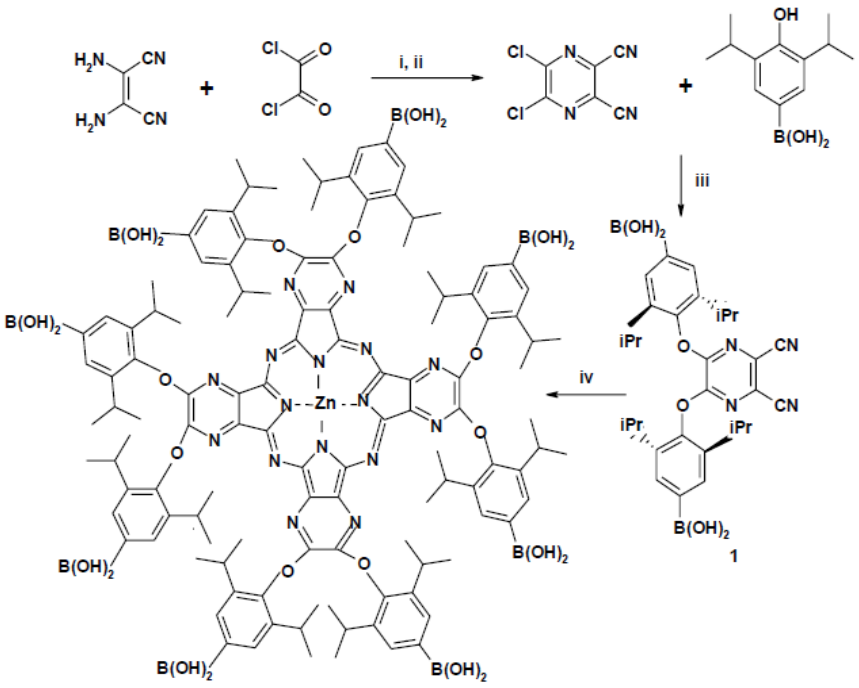

Scheme 1: Reagents and condition; (i) 1,4-Dioxane; 50 °C, (ii) $SOCl_2$, dioxane, 100 °C (iii) CH_3CN; 78 °C, (iv) Dry quinoline, appropriate metal salt for Zn.

Synthesis of Zn-2,3,9,10,16,17,23,24–octa(2,6-diisopropylphenoxy) azaphthalocyanine Aza-Pc

This compound was obtained as green solid in (55 %) yield, mp>300 °C. Elemental analysis (Found: C, 72.27; H, 7.27; N, 11.08 %. $C_{120}H_{136}N_{16}O_8Zn$ requires C, 72.48; H, 6.87; N, 11.27 %) IR υ (KBr)/cm^{-1}: 3440 (ArH); UV (abs. THF): λ/nm, (ε) = 615 (67554), 560 (11928), 383 (15904), 336 (39760); δH ($CDCl_3$, 400 MHz, 25 °C), 1.31 (96H, d), 3.30 (16H, m), 7.44 (16H, d), 7.58 (8H, t); MS: m/z (MALDI) =1986. **Q**-band shape and positions are strongly affected by Aza-Pc concentration owing to the tendency to form dimers and higher aggregates. It is apparent that the number, type and positions of the substituent groups have a profound influence, not only on the solubility of the derivatives, but also on the arrangements of the Aza-Pc within the solid state, thus influencing the **Q**-band absorption position.[19] It is difficult to glean any structure-electronic absorption[20] trends with respect to either the substituents or the metal occupying the cavity.[21] The synthesis of an Aza-Pc series,[22] which differs in the number of attached linearly condensed benzo rings showed that the characteristic electronic transitions of Aza-Pc are similar to the related phthalocyanines. The electronic transition gaps between their LUMO (eg) and HOMO (a_{1u}) energy levels are larger than the corresponding phthalocyanines with **Q**-band for Pcs (680-700nm) and (620-630nm) for Aza-Pc. The reason could be that the conjugated macrocyclic ring of Aza-Pc is less planar than the phthalocyanine core. The Aza-Pcs strong visible absorption band **Q**-band, shifted from it's normal position (620-630nm) into the near-IR by adding alkoxy groups or by extending the π-orbital conjugation as a result of red-shift **Q**-band.[23,24]

Synthesis of CQDs

In a typical experiment, 40mL of extract lemon juice (ivory white solution) was put into a Teflon-lined stainless steel autoclave for hydrothermal treatment at 120 to 280°C for 12 h. After the reaction, the autoclave was naturally cooled to room temperature. During this hydrothermal process, ivorywhite solution changed to dark brown solution, indicating the formation of CQDs. These carbon dots were then purified to remove the

larger nanoparticles by 2 μm filter paper microstructure and particles size distribution of it.

Relative orientation of transition dipole moment

The differences in the absorption spectra obtained from solid-state Aza-Pc materials compared with isolated molecular ^{1}H NMR spectra can be explained on the bases of the interactions between the transition moments of adjacent molecules (dimers interactions). For cofacial dimers, transitions to the higher energy levels are allowed as shown in Figure 2, and the **Q**-band is blue-shifted relative to its position in the isolated molecular spectrum. The lower energy exciting interaction produces no net dipole change and therefore no light absorption. Aza-Pc with parallel orientation results a red-shift as expected. Dimers that are in a tilted arrangement (a herringbone arrangement) relative to one another leads to strong Davydov splitting giving bands both at higher and lower wavelengths relative to **Q**-band of the solution phase isolated molecular.[24] **Q**-band owing to the dipoles cancel each other neither in the higher nor in the lower energy configurations.

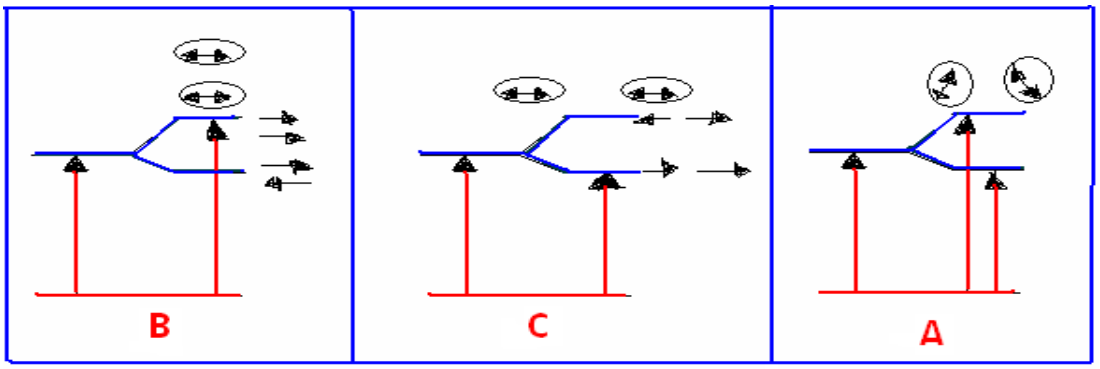

Figure 2: Model of exciting splitting of the Q-band between the two Metal Aza-Pc molecules in (b) face to face (c) edge-to edge (a) tilted arrangements.

Bathochromic shift (red-shift) of the **Q**-band results from raising the energy level of the HOMO by the substitution with E.D.G or as in naphthalocyanines is shifted to the red by approximately 90 and 170 nm respectively.

Split Q-bands obtained from Aza-Pc

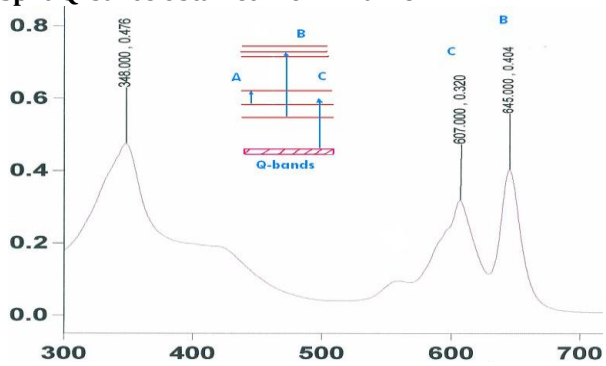

Figure 3: UV/VIS absorption and schematic energy diagrams of Aza-Pcs.

SEM and HRTM analysis

SEM images of Aza-Pc of different Zn nano-sizes confirm the presence of irregular particles of different sizesas shown in Figures 4 and 5. The network polymer structure composed of nanoframes arranged in an ordered manner and show well defined microstructure. Like other microporous carbons, the synthesized network Aza-Pc was found to be stable under the experimental condition which is another indication of the high stability of such materials.

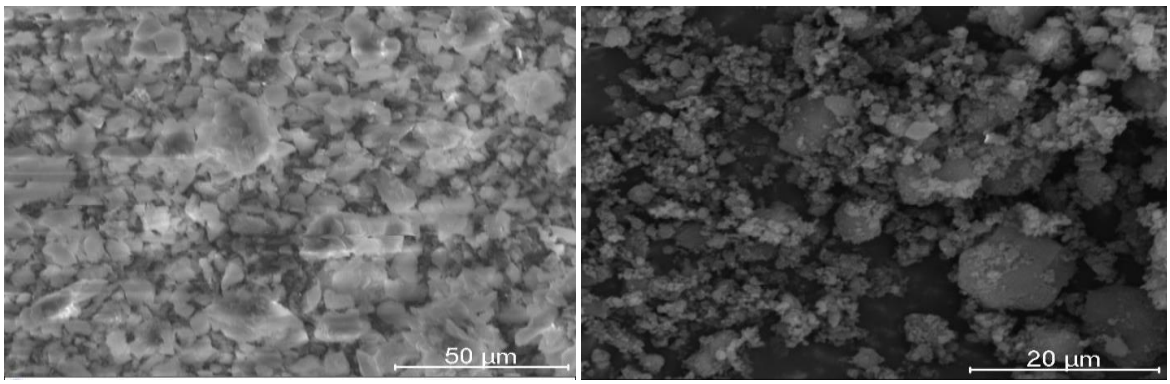

(a) **(b)**

Figure 4: SEM images (a) of Az-Pc of Zn 20 nm and (b) of Az-Pc of 30 nm.

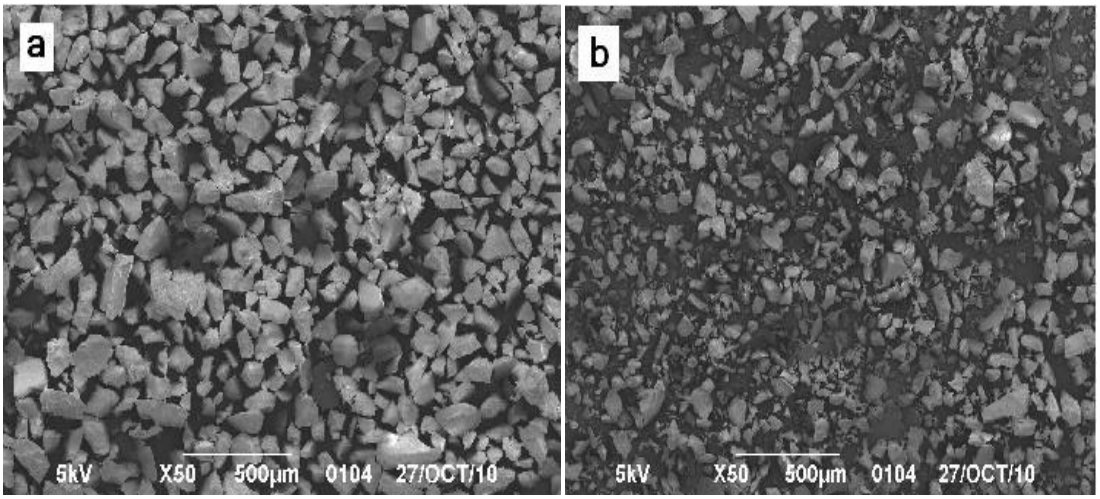

Figure 5: SEM (a) of Az-Pc of Zn 20 nm and (b) of Az-Pc of 30 nm.

The (HRTEM) operating at 300 kV was used to confirm the microstructure of the Az- Pc of 10 nm and the presence of nonporous observed at the area of investigation as shown in Figure 6.

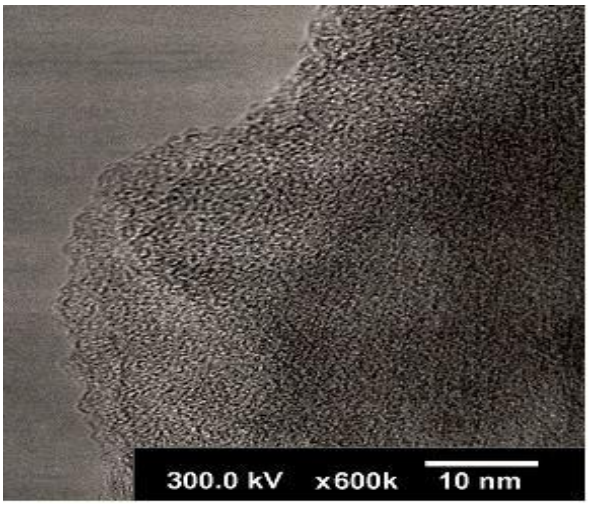

Figure 6: HRTEM image of Az-Pc illustrates its porosity (Wormhole structure), homogeneity, and structural stability under the experimental condition (300 kV). The pore dimensions in good agreement with the micropore size distribution as calculated by the (HK).

Suggested Antiviral Assay of of Antiviral Az-Pcs-CQDs

The antiviral activity of Az-Pcs-CQDs with different Zn nano-size need to be evaluated on Huh-7 cell monolayers infected with COVID-19. Addition of Az-Pcs- CQDs after 1 h infection and further incubation for 6 h at 37 expected to show no inhibition. with COVIDs. CQDs are in this context speculated to be pseudolectins, targeting the S protein of COVIDs via a lectin− carbohydrate binding mechanis.

CONCLUSION

The viral infection cycle produces important biological and structural changes in the host cell, resulting in cell damage. The possibility to interfere with viral attachment to cells as well as viral replication to reduce viral infection and spreading is an appropriate antiviral approach. These CQDs were shown to interfere significantly with COVID-19 infection in a concentration-dependent manner. The presence of boronic acid functions proved to be vital for covering CQDs with antiviral activity Mechanistic studies suggest that the particles are acting at the early state of virus infection through the inhibition of entry that could be due to inhibition of protein S- receptor interaction with the host cell membrane. These results are extremely encouraging to replace currently used antiviral agents such a ribavirin and IFN known to have major side effects. such as confusion, short-term memory loss, deficits in executive functions, as well as extrapyramidal effects. Further experimental confirmations are required if this approach can be extrapolated to other coronaviruses, notably to the clinically relevant MERS-CoV, to validate the potential of these nanostructures as alternative anti-MERS therapeutics and approaches to confront this severe and life-threatening disease. Also, how such particles work in vivo has to be shown in the future.[25]

REFERENCES

1. Alivisatos, P. Nat. Biotechnol, 2004; 22: 47.
2. West, J. L.; Halas, N. J. Curr. Opin. Biotechnol, 2000; 11: 215.
3. Parak, W. J.; Gerion, D.; Pellegrino, T.; Zanchet, D.; Micheel, C.; Williams, S. C.; Boudreau, R.; Le Gros, M. A.; Larabell, C. A.; Alivisatos, A. P. Nanotechnology, 2003; 14, R15.
4. Chan, W. C. W.; Maxwell, D. J.; Gao, X.; Bailey, R. E.; Han, M.; Nie, S. Curr. Opin. Biotechnol, 2002; 13: 40.
5. Drummund, T. G.; Hill, M. G.; Barton, J. K. Nat. Biotechnol, 2003; 21: 1192.
6. Willner, I.; Patolsky, F.; Weizmann, Y.; Willner, B. Talanta, 2002; 56: 847.
7. Niemeyer, C. M. Angew. Chem., Int. Ed., 2001; 40:

4128.
8. Lander, E. S. Nat. Biotechnol, 1999; 21: 3.
9. Duggan, D. J.; Bitttner, M.; Chen, Y.; Meltzer, P.; Trent, J. M
10. Tyagi, S.; Kramer, F. R. Nat. Biotechnol, 1996; 14: 303.
11. Fang, X.; Liu, X.; Schuster, S.; Tan, W. J. Am. Chem. Soc., 1999; 121: 2921.
12. Saiki, R. K.; Scharf, S.; Faloona, F.; Mullis, K. B.; Horn, G. T.; Erlich, H. A.; Arnheim, N. Science, 1985; 230: 1350.
13. Kirk, B. W.; Feinsod, M.; Favis, R.; Kliman, R. M.; Barany, F. Nucleic Acids Res., 2002; 30: 3295.
14. Detectable concentration varies with target protein, but they are typically in the pM range.
15. S. Y. Lim, W. Shen, and Z. Gao, "Carbon quantum dots and their applications," Chemical Society Reviews, 2015; 44(1): 362–381.
16. G. Hong, S. Diao, A. L. Antaris, and H. Dai, "Carbon nanomaterials for biological imaging and nanomedicinal therapy," Chemical Reviews, 2015; 115(19): 10816–10906.
17. B. T. Hoan, P. Van Huan, H. N. Van et al., "Luminescence of lemon-derived carbon quantum dot and its potential application in luminescent probe for detection of Mo $^{6+}$ ions," Luminescence, 2018; 33(3): 545–551.
18. Y. Xu, C. J. Tang, H. Huang et al., "Green synthesis of fluorescent carbon quantum dots for detection of Hg^{2+}," Chinese Journal of Analytical Chemistry, 2014; 42(9): 1252–1258.
19. Mckeown, N.B. Solution characteristics. Phthalocyanine Materials Synthesis, Structure and Function, 1998; 4: 88-92. Cambridge University.
20. Yakushi, K., Hiejima, T., Materials and Measurements in Molecular Electronics, 81: 203. New York, 1996.
21. Matthew J., Fuchter, L., Scott Beall, Sven M., Baum, and Antonio G. Synthesis of porphyrazine-octaamine. Tetrahedron, 2005; 61: 6118-6130.
22. Newcombe G.R., Moorefield. C.N., and Vogtle F. Dendritic Molecules: Concepts, Syntheses and Perspectives. VCH: Weinheim, 1996.
23. Lukyanets, E.A., Phthalocyanines aggregation property. J. Porphyrins Phthalocyan, 1999; 3: 424.
24. Christian, G., Claessens, Werner, J. Blau, Michael, H. Roeland, J., and Tomas, T. Phthalocyanines and Phthalocyanine Anolgues: The Quest for Applicable Optical Properties. Monatshefte fur Chemie, 2001; 132: 3-11.
25. O Keefe, B. R.; Giomarelli, B.; Barnard, D. L.; Shenoy, S. R.; Chan, P. K. S.; McMahon, J. B.; Palmer, K. E.; Barnett, B. W.; Meyerholz, D. K.; Wohlford-Lenane, C. L.; McCray, P. B. Broad-Spectrum In Vitro Activity And In Vivo Efficacy Of The Antiviral Protein Griffithsin Against Emerging Viruses Of The Family Coronaviridae. J. Virol., 2010; 84: 2511−2521.